ADVANCED FUNCTIONAL MATERIALS

Supporting Information

for *Adv. Funct. Mater.*, DOI: 10.1002/adfm.201904020

Constructing Conductive Interfaces between Nickel Oxide Nanocrystals and Polymer Carbon Nitride for Efficient Electrocatalytic Oxygen Evolution Reaction

Chengan Liao, Baopeng Yang, Ning Zhang, Min Liu, Guoxin Chen, Xiaoming Jiang, Gen Chen, Junliang Yang, Xiaohe Liu,* Ting-Shan Chan, Ying-Jui Lu, Renzhi Ma,* and Wei Zhou*

Supporting Information

Constructing Conductive Interfaces between Nickel Oxide Nanocrystals and Polymer Carbon Nitride for Efficient Electrocatalytic Oxygen Evolution Reaction

Chengan Liao, Baopeng Yang, Ning Zhang, Min Liu, Guoxin Chen, Xiaoming Jiang, Gen Chen, Junliang Yang, Xiaohe Liu,* Ting-Shan Chan, Ying-Jui Lu, Renzhi Ma*, Wei Zhou*

C. Liao, B. Yang, Prof. N. Zhang, Prof. G. Chen, Prof. X. Liu
School of Materials Science and Engineering, Central South University, Changsha, Hunan 410083, China
E-mail: nzhang@csu.edu.cn, liuxh@csu.edu.cn

Prof. R. Ma, Prof. Wei Zhou
International Center for Materials Nanoarchitectonics (MANA), National Institute for Materials Science (NIMS), 1-1 Namiki, Tsukuba, Ibaraki 305-0044, Japan
E-mail: ma.renzhi@nism.go.jp

Prof. J. Yang, Prof. M. Liu
School of Physical Science and Electronics, Central South University, Changsha, Hunan 410083, China

Prof. G. Chen
Ningbo Institute of Materials Technology & Engineering, Chinese Academy of Sciences, No. 1219 Zhongguan West Road, Zhenhai District, Ningbo, Zhejiang 315201, China

Prof. X. Jiang
State Key Lab of Structural Chemistry, Fujian Institute of Research on the Structure of Matter, Chinese Academy of Sciences, Fuzhou, Fujian 350002, China

T. Shan Chan, Y. J. Lu
National Synchrotron Radiation Research Center, Taiwan, 101 Hsin Ann Road, Hsinchu Science Park, Hsinchu 300, Taiwan, China

Experimental Section

Characterization

X−ray diffraction profiles were recorded by a RIGAKU Rint−2000 X−ray diffractometer equipped with graphite monochromatized Cu−Kα radiation (λ=1.54184 Å). The SEM images and EDS spectra of samples were collected on a FE-SEM Quanta 200 FEG field emission scanning electron microscopy. TEM and HRTEM images was recorded by FEI Tecnai G2 F20 field emission transmission electron microscopy operated at 200 kV. The X−ray photoelectron spectroscopy spectra were performed using a Thermo Fisher ESCALAB 250Xi spectrophotometer. The X-ray absorption spectroscopy experiments were performed at the National Synchrotron Radiation Research Center (NSRRC) in Taiwan.

Three-electrodes electrochemical measurement

Electrochemical experiments were measured on a CHI 760E electrochemical workstation in a three-electrode cell and gas flow control systems at room temperature. Hg/HgO (1 M KOH-filled) electrode was used as reference electrode, platinum plat electrode was acted as counter electrode. The rotating ring disk electrode (RRDE) modified with catalyst was used as the working electrode. The catalyst ink was prepared by dispersing a 10 mg catalyst in 1 mL ethanol and 1mL deionized water to form ethanol/water solution. Subsequently, 15 μL Nafion solution (Nafion D-521 5% w/w in water and 1-propano, Alfa Aesar Co. Ltd.) was added to the ink as a proton conducting binder to ensure good adhesion onto the RRDE. To form a homogeneous solution, the catalyst ink was ultrasonic dispersed for 30 min and vigorous stirred for 12h at room temperature. After polishing the electrode with a suspension of alumina, the surface of RRDE (0.07 cm^2) was coated with 4 μL of the catalyst ink to make the catalyst on the working electrode was about 0.285mg cm^{-2}. The pasted catalyst on the working electrode was dried at 60 °C in vacuum for further use. All OER measurements were carried out in 1M KOH electrolyte solution which was purged with high-purity nitrogen about

15 min. All polarization curves were corrected with 95% iR compensation. Cyclic voltammograms (CVs) were performed with 30 cycles to reach the stabilization. The linear sweep voltammetry (LSV) curve was recorded with a scan rate of 10 mV s^{-1} with the rotation rate of 1600 rpm. The current density was normalized to the geometrical surface area and the potentials (vs. Hg/HgO) were corrected to the reversible hydrogen electrode (RHE) according to the equation: $E_{RHE} = E_{Hg/HgO} + 0.059 \times pH + 0.098$. Tafel slope was obtained from the corresponding LSV curves according to the equation: $\eta = a + b*\log j$ (η is overpotential, j is anodic current density, and b is Tafel slope). The electrochemical impedance spectroscopy (EIS) was measured at 1.55 V (vs. RHE) in the frequency range from 10^5 to 0.1 Hz with an amplitude of 5 mV. The cycling stability curve was collected by a chronopotentiometry response in N_2-saturated 1 M KOH solution at the current density of 10 mA cm^{-2} for several hours.

DFT Calculation

To further understand the effect of highly conductive interfaces between nickel oxide nanocrystals and polymer carbon nitride on oxygen evolution reaction, first-principles calculations were carried out by using Vienna Ab initio Simulation Package (VASP). Projector augmented wave (PAW) was adopted to describe electron interactions. The Perdew–Burke–Ernzerhof (PBE) functional of the generalized gradient approximation (GGA) was used as the exchange–correlation function. To simulate NiO nanocluster anchored on g-C_3N_4, firstly, a single layer g-C_3N_4 model was optimized, which construction with a 2×2×1 unit cell with one layer atomic slab and a 15 Å vacuum layer region in the z direction (**Figure S5a**). Then an optimized NiO nanocluster including thirteen Ni atoms and thirteen O atoms was linked with single layer g-C_3N_4 by forming Ni-N bonds (**Figure S5c**). To simulate NiO nanocluster, a similar sphere NiO with a diameter of 8 Å was constructed. And the model of NiO nanocluster had about 10 Å vacuum region in the x, y, and z directions to minimize the

interactions between adjacent image cells by relaxed via the conjugate-gradient method (**Figure S5b**). To confirm the strong correlated electronic states in Ni, the GGA+U method was used. In this study, we used Hubbard U of 3.8 eV for the Ni d-states in the caculations included Ni. During all calculations, the energies change criterion was set to 10^{-4} eV, and the atoms were relaxed until the force acting on each atom was less than 0.01 eV $Å^{-1}$. The plane-wave basis set was within the kinetic cutoff energy of 500 eV for all compute instances. The k-point grids were set to be 3×3×1 for NiO@g-C_3N_4, and the k-point grids for NiO nanocluster was set to be 1×1×1. The adsorption energy of intermediates on the surface of NiO and NiO@g-C_3N_4 were calculated using the following method:

In alkaline conditions, The OER process currently involve four elementary reaction steps:

$$OH^- + * \rightarrow OH^* + e^- \quad (1)$$

$$OH^* + OH^- \rightarrow O^* + H_2O + e^- \quad (2)$$

$$O^* + OH^- \rightarrow OOH^* + e^- \quad (3)$$

$$OOH^* + OH^- \rightarrow O_2 + H_2O + e^- \quad (4)$$

Where * and *X** represent an active site and an adsorbed *X* intermediate (*X*=*OH*, *O*, and *OOH*) on the surface, respectively. Based on the above OER steps, the relevant computational models of intermediates adsorbed on the surface of NiO and NiO@g-C_3N_4 were constructed; the detailed models are presented in **Figure S6**.

Adsorption energy of intermediates (*O**, *OH**, *OOH**) on (*) substrate were determined by the following approach of Nøeskov et al.

$$\Delta E_{OH^*} = E(OH^*) - E(*) - \left(E_{H_2O} - 1/2\, E_{H_2}\right) \quad (5)$$

$$\Delta E_{O^*} = E(O^*) - E(*) - (E_{H_2O} - E_{H_2}) \quad (6)$$

$$\Delta E_{OOH^*} = E(OOH^*) - E(*) - (2E_{H_2O} - 3/2\, E_{H_2}) \quad (7)$$

Where *E*(*), *E*(*HO**), *E*(*O**), and *E*(*HOO**) are the total energies of the pure surface and the adsorbed surface with *HO**, *O**, and *HOO**, respectively, which can be got from the

caculations. E_{H2O} and E_{H2} are the computed energies for the sole H_2O and H_2 molecules, respectively.

The Gibbs free energy changes of intermediates adsorbed on the surface of catalysts were calculated with zero point energy and entropy corrections using the following computational formula:

$$\Delta G_{X^*} = \Delta E_{X^*} + (\Delta ZPE - T\Delta S)_{X^*} \quad (8)$$

Where *ZPE*, *T*, and *S* are the zero point energy, temperature, and entropy, respectively.

The Gibbs free energy changes for steps 1-4 can be expressed as follows:

$$\Delta G_1 = \Delta G_{OH^*} - eU \quad (9)$$

$$\Delta G_2 = \Delta G_{O^*} - \Delta G_{OH^*} - eU \quad (10)$$

$$\Delta G_3 = \Delta G_{OOH^*} - \Delta G_{O^*} - eU \quad (11)$$

$$\Delta G_4 = 4.92[eV] - \Delta G_{OOH^*} - eU \quad (12)$$

Where *U* is the applied voltage, in this study, *U*=0, and the total free energy (ΔG) to form one molecule of O_2 was fixed at the value of 4.92 eV in order to avoid the calculation of the O_2 bond energy, which is difficult to determine accurately within GGA-DFT.

Photovoltaic-Electrocatalytic Water Splitting Evaluation

The photovoltaic-water electrolysis was characterized by an online gas chromatography (GC-2014C, Shimadzu Corp., Japan) which is connected to a closed gas-circulation system with a water splitting reactor (Online-3, Shanghai Boyi Scientific Instrument Co., China). Typically, the anode (the NiO/CN catalyst on Ni foam, 1 cm^2) and cathode (bare Ni foam, 1 cm^2) were installed on a water splitting reactor and connected to a crystalline silicon solar cell. The distance between two electrodes was 2 cm. About 280 mL KOH (1 M) solution was used as electrolyte for water splitting. Then the water splitting reactor and closed gas-circulation system were achieved vacuum state by vacuumizing. A Xe lamp ($400 < \lambda < 800$ nm) was used as the light source and the light intensity can be controlled by adjusting the input current on Xe lamp and/or the distance be between light source and solar cell. A crystalline silicon solar

cell with a total irradiated area of 14.4 cm^2 was applied to convert photo energy to electric energy. A circulating water unit was employed to protect the solar cell from overheating. In addition, a voltmeter was used to monitor the voltage applied to the electrodes. After turn on the Xe lamp, the light intensity was adjusted to keep a working voltage of 2.45 V from solar cell.

Calculation of Solar-to-Hydrogen Energy Conversion Efficiency

As shown in Figure S6, the light intensity of Xe lamp is concentrated on the wavelength range of 400 nm ~ 800 nm. The average integral light intensity measured by the light meter is 0.5411 W cm^{-2}. The irradiated area for the silicon solar cell is 14.4 cm^2. The standard molar enthalpy of combustion for H_2 is -285.84 KJ mol^{-1}. The yield of H_2 during the first hour is 5249.9 μmol. The calculation steps are as following:

Input:

Solar energy (J) = light intensity (W cm^{-2}) × illumination area (cm^2) × time (s) = 0.5411 W cm^{-2} × 14.4 cm^2 × 3600 s = 28049.1 J =28.0491 kJ

Output:

H_2 energy (kJ) = standard molar enthalpy of combustion (kJ mol^{-1}) × H_2 moles (mol) = 285.84 kJ mol^{-1} × 5249.9 × 10^{-6} mol = 1.50 kJ

Solar-to-Hydrogen energy conversion efficiency = H_2 energy (kJ) / Solar energy (kJ) = 1.50 / 28.049 = 5.35%

Calculation of the Faraday Efficiency

Faraday efficiency was defined as the ratio between the actual and theoretical amount of the product. The total charge ($Q = I \times t$) passed during the reaction was divided by $n \times F$ (n is the number of electron transfer, F is the Faraday constant) to get the theoretical gas yield. m is the actual moles of the product (5249.9 μmol during the first hour). The calculation process for the Faraday efficiency is as following:

Faraday efficiency = actual gas yield / theoretical gas yield = m / [($I \times t$) / ($n \times F$)] = ($m \times n \times F$) / ($I \times t$) = (5249.9 × 10^{-6} mol × 2 × 96485 C mol^{-1}) / (284.8 × 10^{-3} A × 3600 s) = 98.81%

Additional Tables and Figures

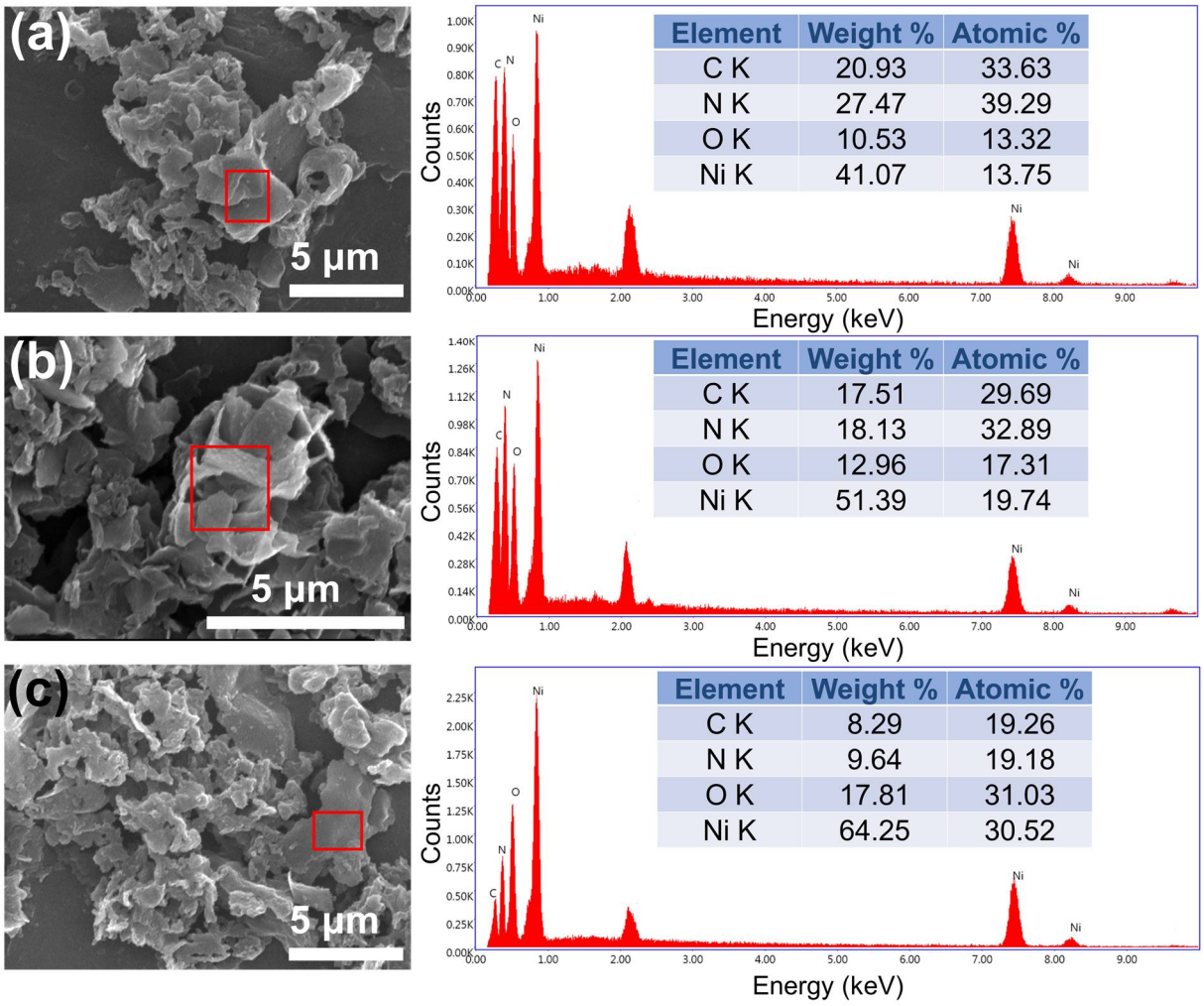

Figure S1 The SEM images and EDS spectra of (a) NiO/CN-1:1, (b) NiO/CN-2:1, and (c) NiO/CN-5:1.

Table S1 The value of R_s, R_{ct},and R_{oad} were obtained by fitting the EIS curves

Products	R_s (Ω)	R_{ct} (Ω)	R_{oad} (Ω)
CN	10.0	230.6	169.2
NiO	9.6	49.2	72.5
NiO/CN-1:1	9.8	32.6	40.1
NiO/CN-2:1	9.8	13.4	28.6
NiO/CN-5:1	10	22.9	32.6

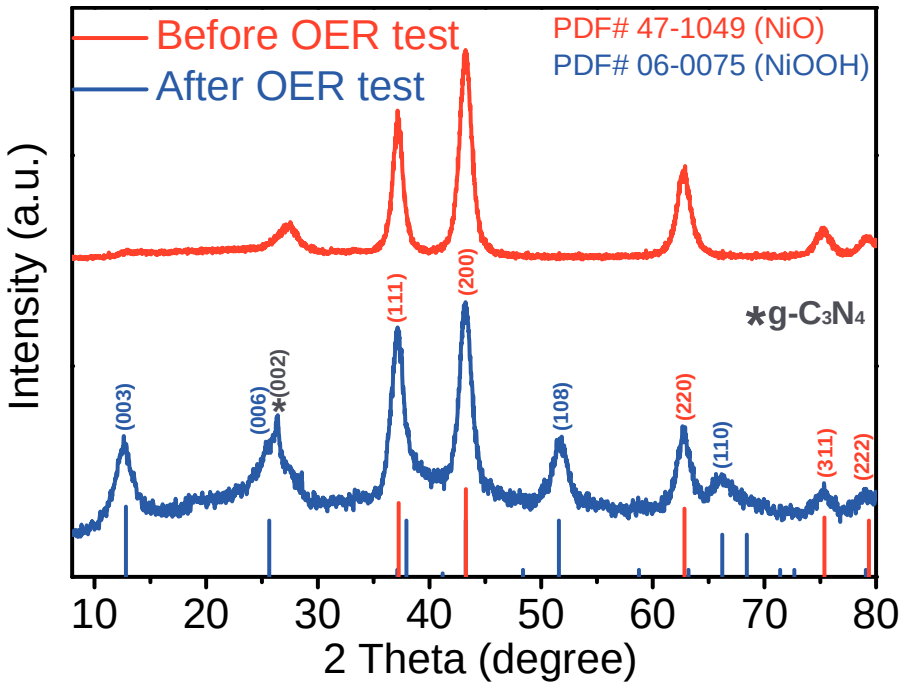

Figure S2 XRD patterns of NiO/CN-2:1 before and after OER test.

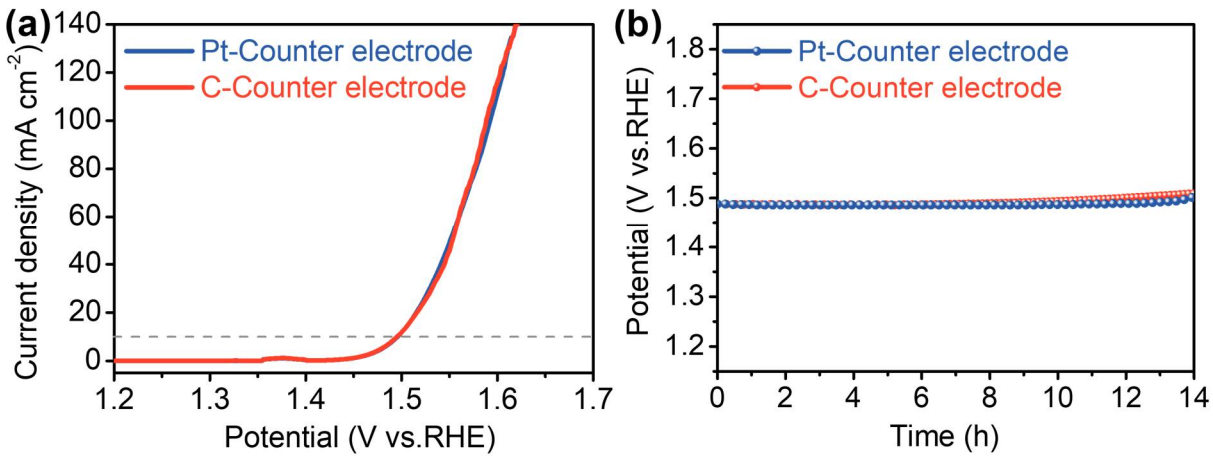

Figure S3 OER performance of the NiO/CN-2:1 catalyst by using Pt plat and carbon rod as counter electrodes in 1M KOH: (a) Linear sweep voltammetry curves of NiO/CN-2:1 at a scan rate of 10 mV s^{-1}; (b) chronopotentiometry curves of NiO/CN-2:1 under a constant current density of 10 mA cm^{-2}.

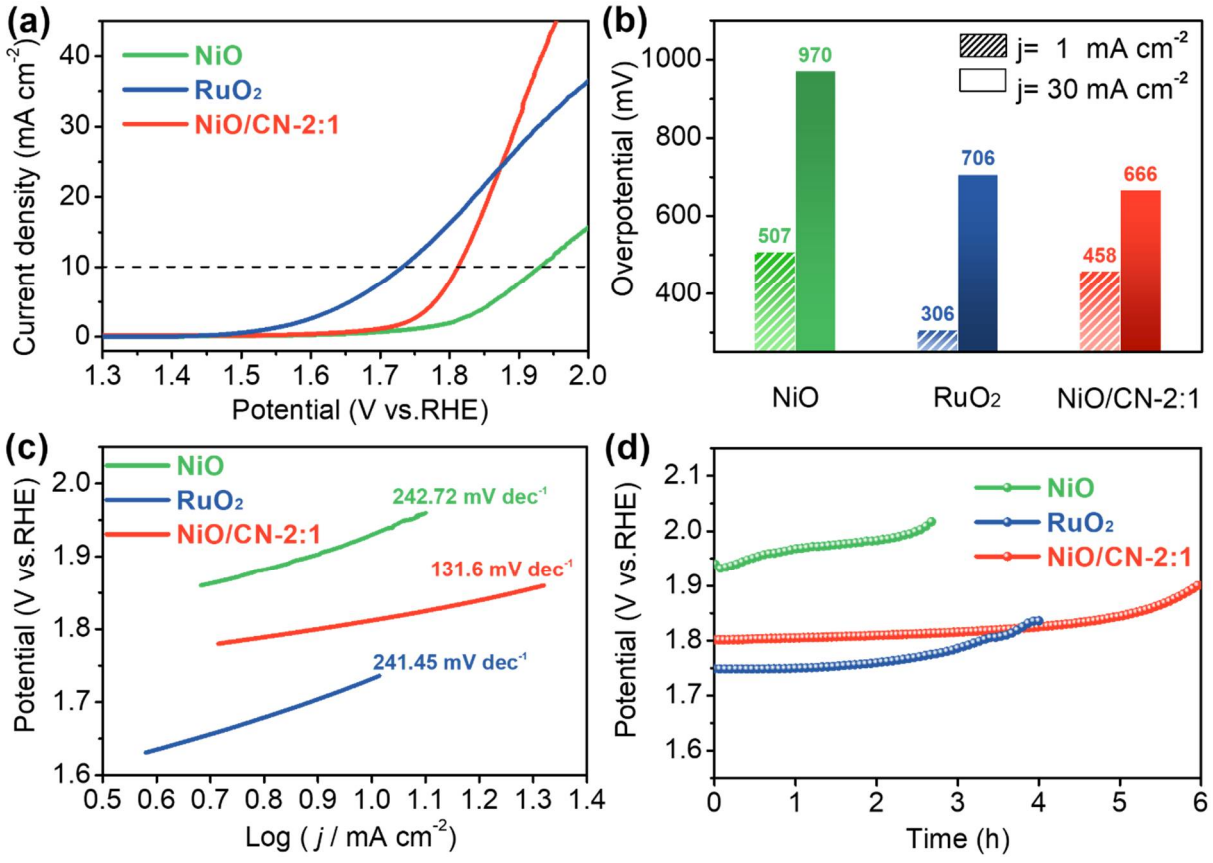

Figure S4 OER performance of the NiO, NiO/CN, and commercial RuO_2 catalysts in 0.05M PBS: (a) polarization curves at a scan rate of 10 mVs^{-1} and (b) the calculated overpotentials at

1 mA cm^{-2} and 30 mA cm^{-2}; (c) Tafel plots derived from corresponding polarization curves; (d) chronopotentiometry curves under a constant current density of 10 mA cm^{-2}.

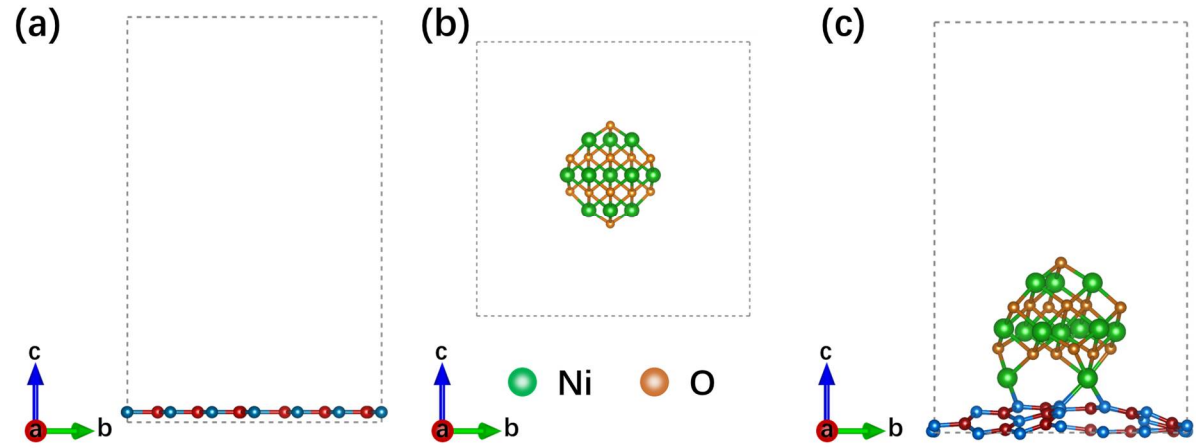

Figure S5 Atomic structure of (a) CN, (b) NiO, and (c) NiO/CN for DFT calculations.

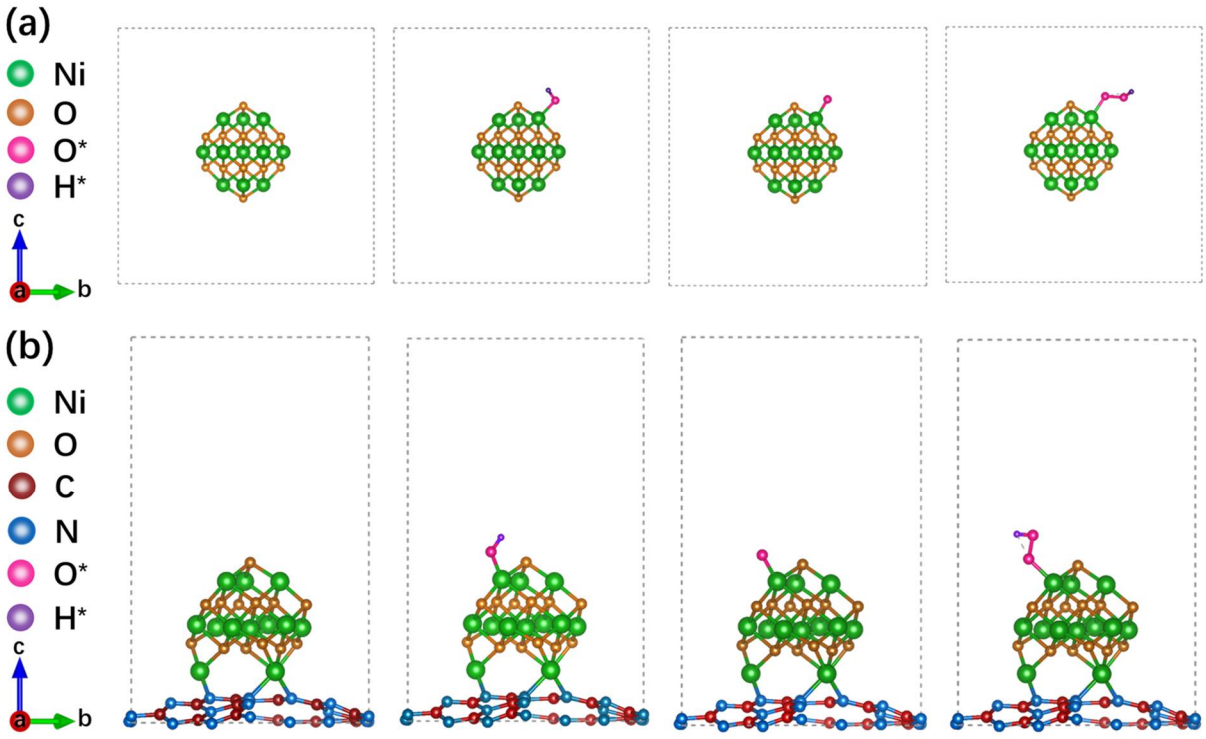

Figure S6 The optimized atomic models for intermediates adsorptions on (a) NiO and (b) NiO/CN

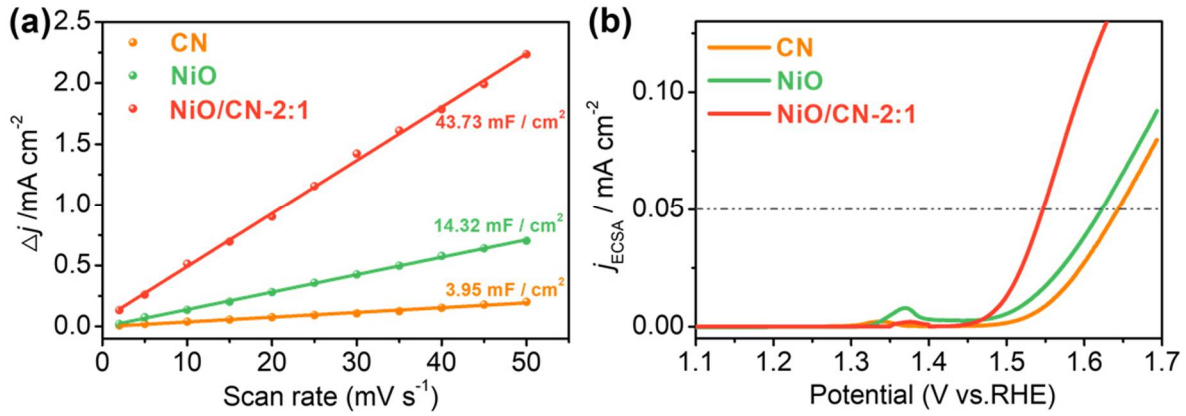

Figure S7 (a) current density difference plotted against scan rates and (b) LSV curves normalized with ESCA for NiO, NiO/CN-2:1, and CN.

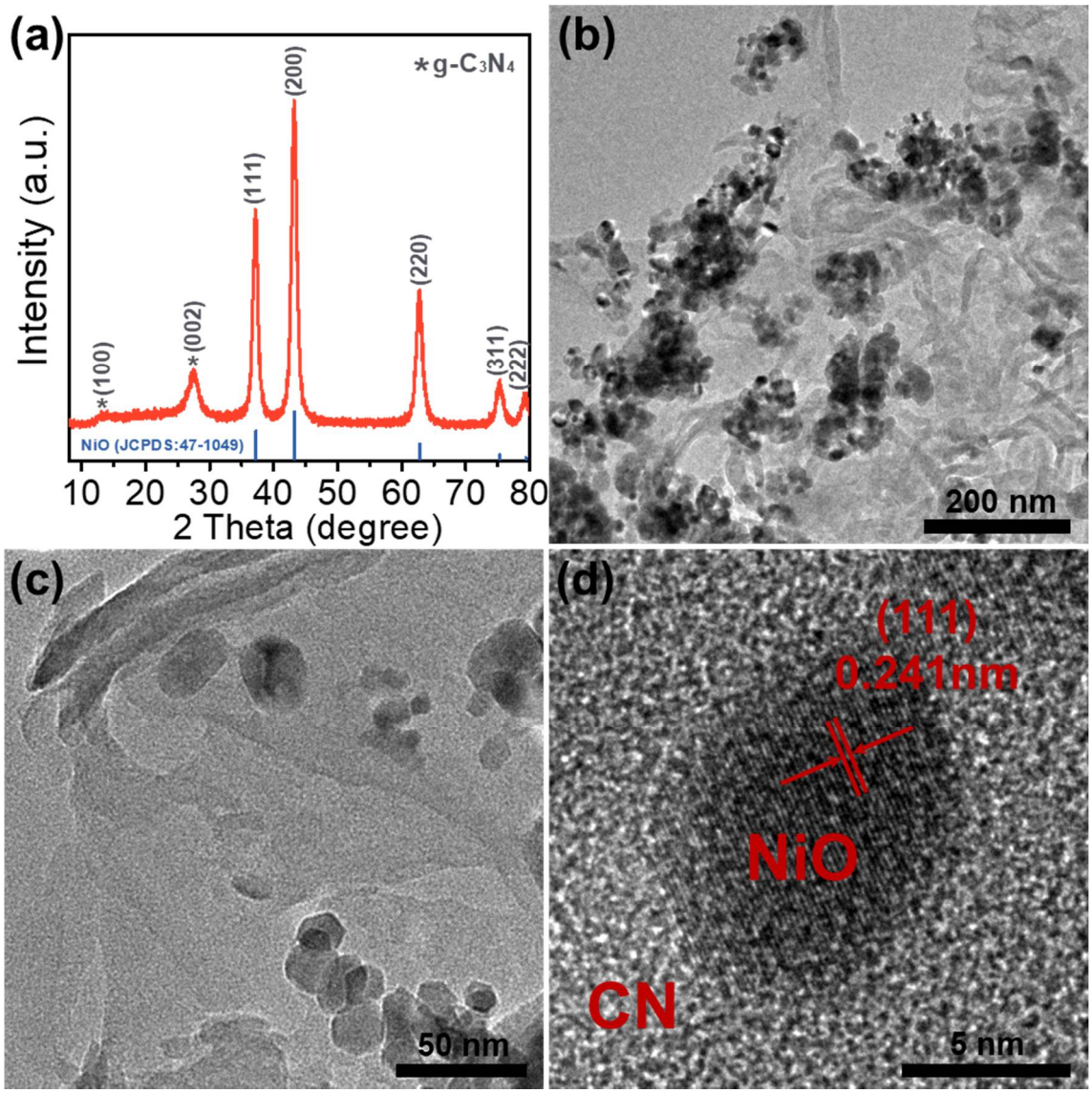

Figure S8 (a) The XRD pattern and (b-d) TEM images of NiO/CN-Control.

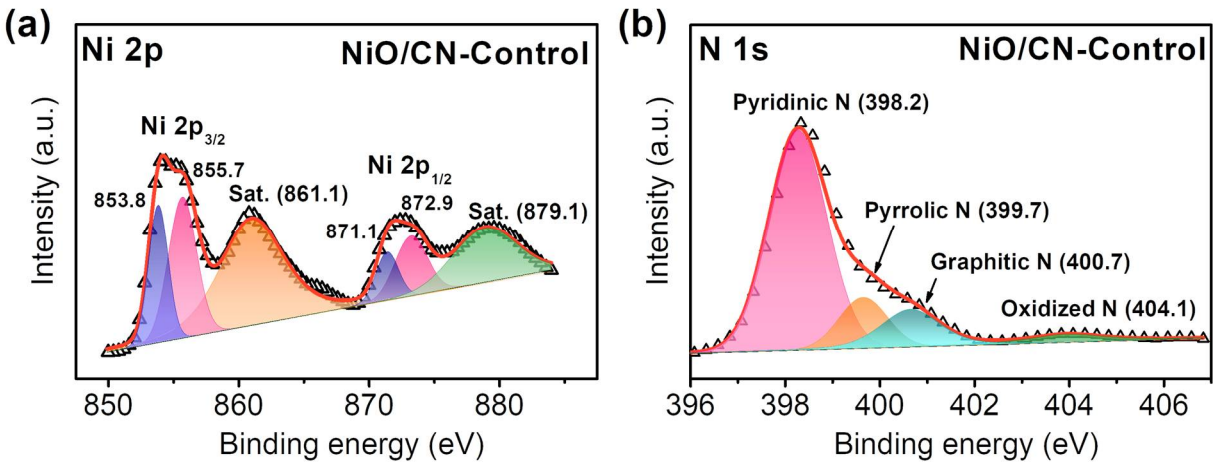

Figure S9 (a) Ni 2p and (b) N 1s XPS spectra of the NiO/CN-Control.

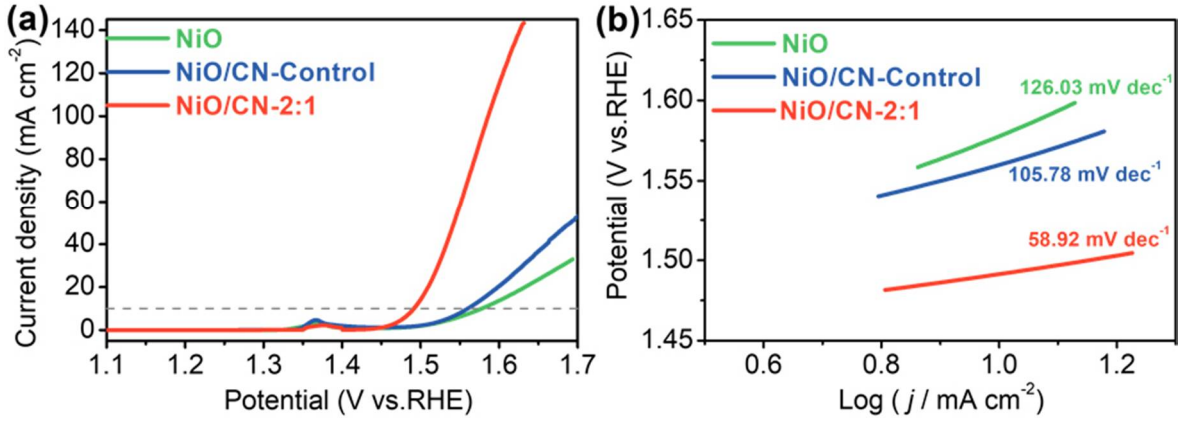

Figure S10 Electrocatalytic OER performance of NiO, NiO/CN-Control, and NiO/CN-2:1 in 1M KOH: (a) iR-corrected LSV curves and (b) Tafel plots.

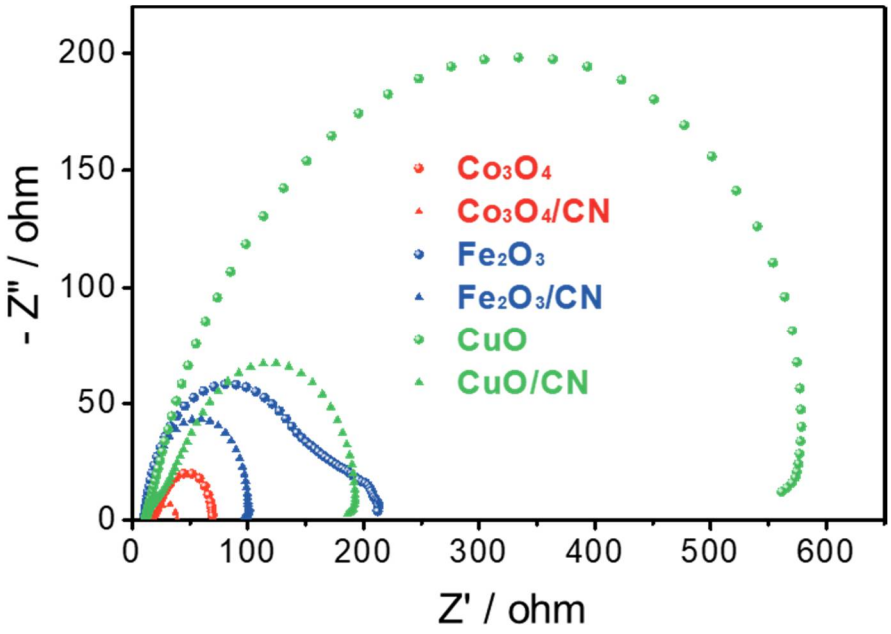

Figure S11 EIS of transition metal oxides CN supported Co_3O_4, Fe_2O_3, and CuO electrocatalysts in 1M KOH.

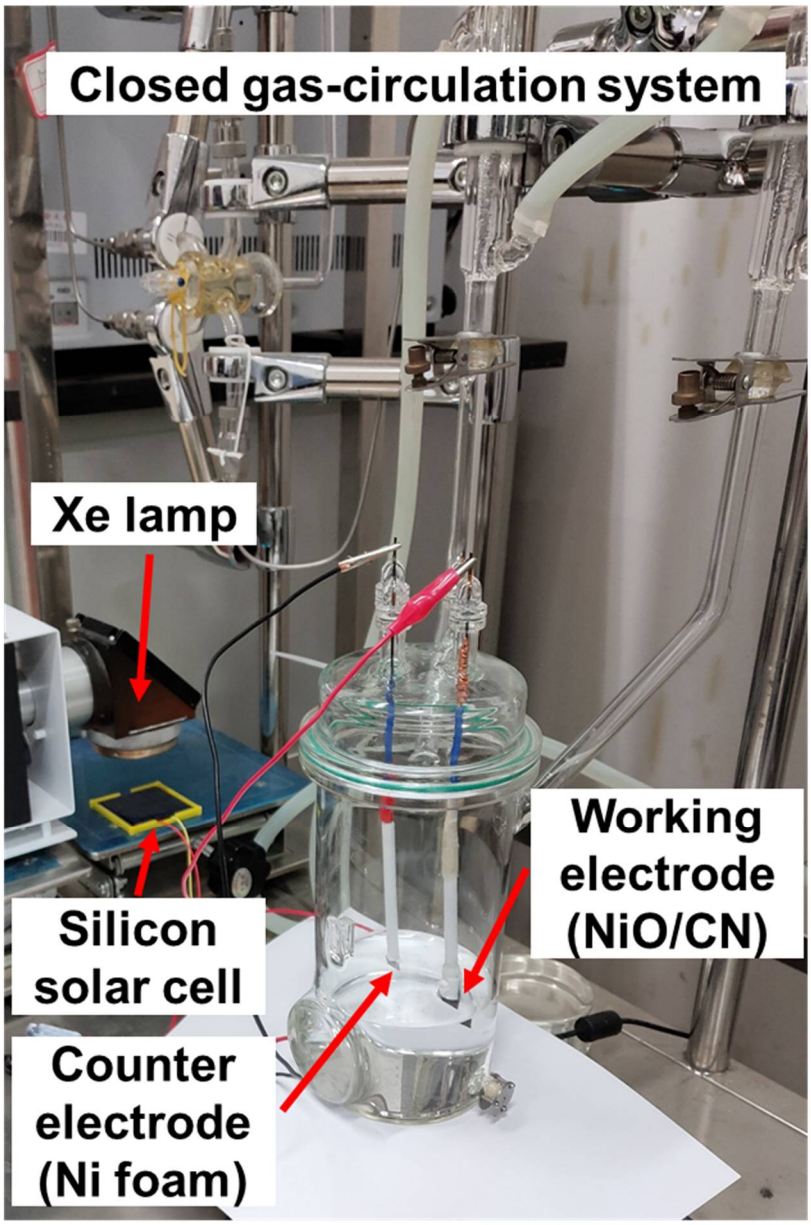

Figure S12 The photograph of photovoltaic-electrocatalytic water splitting system.

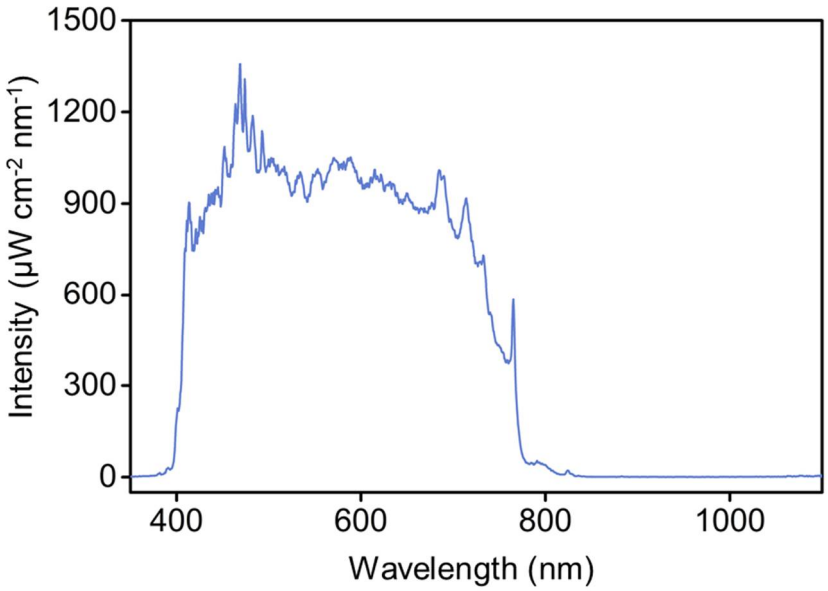

Figure S13 Irradiative spectrum of the Xe lamp (the major intensity is concentrated on the range of 400 nm < λ < 800 nm).

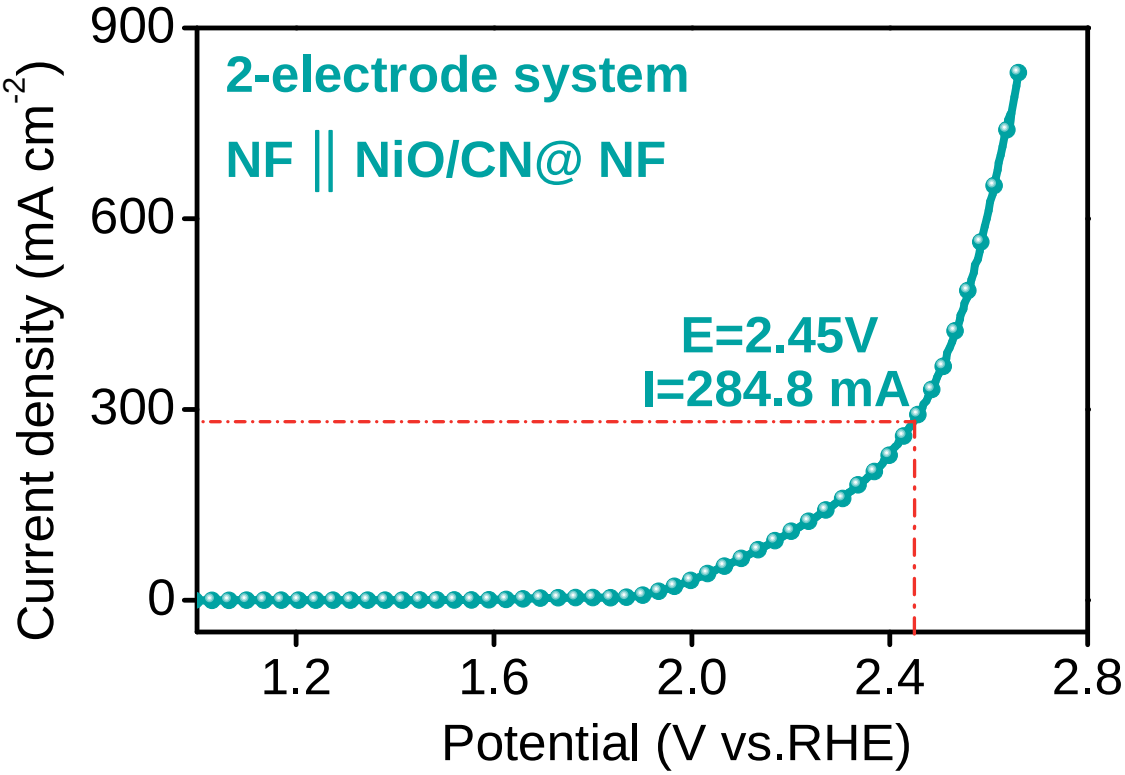

Figure S14 Linear sweep voltammetry curve of the two-electrode system.